Electronic Supplementary Information

Excellent Chirality Transcription in Two-Component Photochromic Organogels Assembled through *J*-Aggregation

Suman K. Samanta,[a] Santanu Bhattacharya*[a,b]

[a]*Department of Organic Chemistry, Indian Institute of Science, Bangalore-560012, India. Fax: +91-80-23600529; Tel: +91-80-22932664; E-mail: sb@orgchem.iisc.ernet.in*

[b]*Chemical Biology Unit, Jawaharlal Nehru Centre for Advanced Scientific Research, Bangalore-560064, India.*

Table of Contents

(a) Experimental Section

Materials and Methods. All reagents, starting materials and silica gel for TLC and column chromatography were obtained from the best known commercial sources and were used without further purification. Solvents were distilled and dried prior to use. FT-IR spectra were recorded on a Perkin-Elmer FT-IR Spectrum BX system and were reported in wave numbers (cm^{-1}). ^{1}H and ^{13}C-NMR spectra were recorded in Bruker-400 Avance NMR spectrometer. Chemical shifts were reported in ppm downfield from the internal standard, tetramethylsilane. Mass spectra were recorded on Micromass Q-TOF Micro TM spectrometer.

Synthesis and Characterization

Pyridine-end *p*-phenylenevinylene analogues (**1** and **2**) were synthesized in a single-step process involving Wittig reaction as summarized in Scheme S1. Both the compounds were characterized by FT-IR, ^{1}H-NMR, ^{13}C-NMR, Mass spectroscopy and also by elemental analysis. An all-trans configuration of the vinyl moieties in the final compounds were confirmed from the coupling constants in the respective ^{1}H-NMR spectrum recorded in $CDCl_3$ (J = ~16 Hz for both). Compound **3** and **5** were prepared as per the previous reported procedure.[S1,S2] Compound **4** was purchased from commercially available source (Sigma-Aldrich) and the precursor **6** has been prepared according to a literature procedure.[S3]

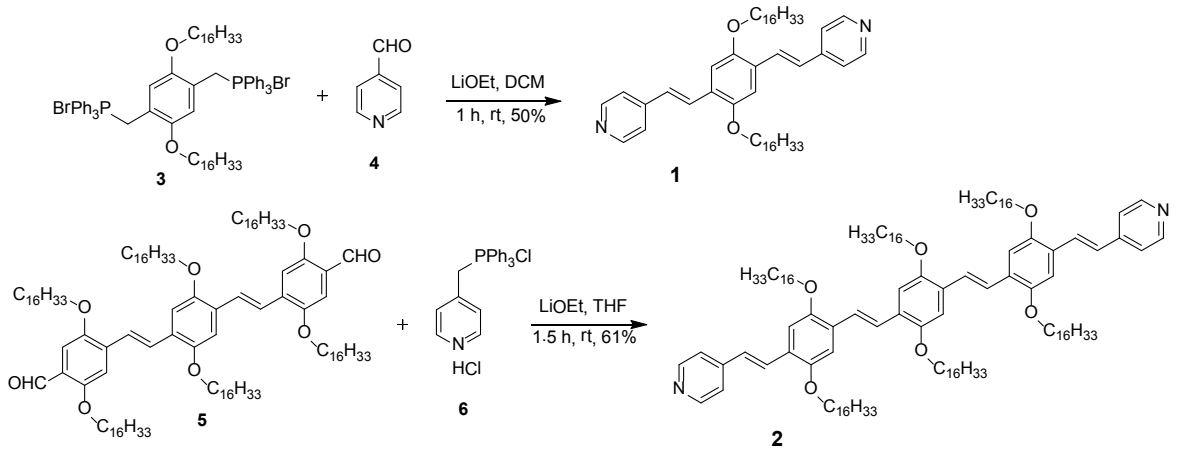

Scheme S1. Reaction scheme showing the routes to the preparation of **1-3**.

Synthesis of 1. The precursor **3** was dissolved in dry dichloromethane and 4-pyridine carboxaldehyde (**4**, 2.2 eq.) was added dropwise and stirred at ice-cold condition. Then into

this solution lithium ethoxide (40 eq) was added under inert atmosphere (N_2) and the mixture was stirred at room temperature for 1 h. The reaction was quenched by adding 2 mL of 3M HCl. The product was then extracted with chloroform and washed with water for several times. Pure product was isolated as a yellow amorphous solid after column chromatography using 15% ethyl acetate in hexane mixture. Yield = 50 %; FT-IR (Neat): $\bar{\upsilon}_{max}$ = 2915, 2851, 1595, 1471, 1324, 1266, 1210, 1046, 963, 845, 798 cm^{-1}. ^{1}H-NMR (400 MHz, $CDCl_3$) δ (ppm) 0.85-0.89 (t, 6 H, CH_3), 1.25-1.41 (m, 48 H, CH_2), 1.52-1.54 (m, 4 H, CH2), 1.86-1.90 (m, 4 H, O-CH_2-CH_2), 4.05-4.08 (t, 4 H, O-CH_2), 7.05-7.09 (d, J = 16.4, 2 H, vinylic), 7.12 (s, 2 H, aromatic), 7.36-7.38 (d, J = 5.9, 2 H, aromatic), 7.64-7.68 (d, J = 16.4, 2 H, vinylic), 8.56- 8.58 (d, J = 5.9, 2 H, aromatic). ^{13}C-NMR (100 MHz, $CDCl_3$) δ (ppm) 14.11, 22.68, 26.26, 29.35, 29.41, 29.61, 29.64, 29.68, 31.91, 69.48, 110.94, 120.83, 126.64, 126.68, 127.85, 145.08, 150.17, 151.57. TOF-MS: calcd for $C_{52}H_{80}N_2O_2$: 765.6298 (M+H); found: 765.6296. Anal. Calcd. For $C_{52}H_{80}N_2O_2$: C, 81.62; H, 10.54; N, 3.66, found: C, 81.84; H, 10.25; N, 4.17.

Synthesis of 2. The precursors **5** and **6** were dissolved in dry tetrahydrofuran (mole ratio 1:2.2 respectively) and stirred at ice-cold condition. Lithium ethoxide (40 eq) was added into this solution under inert atmosphere (N_2) and the mixture was stirred at room temperature for 1.5 h. Then the reaction was quenched by adding 2 mL of 3M HCl. The product was extracted with chloroform and washed with water for several times. Pure product was isolated as red amorphous solid after column chromatography. Yield = 61%; FT-IR (Neat): $\bar{\upsilon}_{max}$ = 2918, 2847, 1595, 1459, 1420, 1252, 1205, 1064, 1016, 963, 847, 798, 717 cm^{-1}. ^{1}H NMR (400 MHz, $CDCl_3$) δ (ppm) 0.85-0.88 (m, 18 H, CH_3), 1.24-1.39 (m, 144 H, CH_2), 1.50-1.58 (m, 12 H, CH2), 1.86-1.91 (m, 12 H, O-CH_2-CH_2), 4.04-4.09 (m, 12 H, O-CH_2), 7.03-7.07 (d, J = 16.4, 2 H, vinylic), 7.11 (s, 2 H, aromatic), 7.15 (s, 2 H, aromatic), 7.17 (s, 2 H, aromatic), 7.36-7.39 (d, J = 5.7, 2 H, aromatic), 7.46-7.50 (d, J = 16.5, 2 H, vinylic), 7.51-7.55 (d, J = 16.5, 2 H, vinylic), 7.66-7.70 (d, J = 16.4, 2 H, vinylic), 8.55- 8.57 (d, J = 5.3, 2 H, aromatic). ^{13}C NMR (100 MHz, $CDCl_3$) δ (ppm) 14.08, 22.68, 23.31, 26.25, 26.33, 26.35, 29.36, 29.49, 29.55, 29.66, 29.71, 29.74, 30.31, 31.92, 35.86, 61.88, 69.38, 69.50, 69.65, 72.31, 110.40, 110.67, 111.21, 120.81, 123.23, 124.30, 125.16, 125.66, 127.49, 128.32, 129.13, 145.56, 149.91, 150.98, 151.20, 151.66, 170.81. MALDI-TOF: calcd for $C_{132}H_{220}N_2O_6$: 1931.169; found: 1931.719. Anal. Calcd. For $C_{132}H_{220}N_2O_6$: C, 82.10; H, 11.48; N, 1.45, found: C, 81.87; H, 11.32; N, 1.29.

(b) Experimental Procedures

General Procedure for the preparation of 1+TA and 2+TA complexes. Either compound **1** or **2** was dissolved in chloroform and stirred at room temperature. In another vial 1 equivalent of either L-TA or D-TA or M-TA was dissolved separately in ethanol and was added into the chloroform solution of either **1** or **2**. The mixture was stirred at room temperature for 1 h. Then all the solvents were removed under vacuum to give a reddish-orange product.

Gelation Studies. For the gelation studies, a weighed amount of a particular compound or its mixture with TA in a vial was added an excess of the chosen solvent. The resulting mixture was heated till the solid was completely dissolved in a stoppered vial. The clear solution was left to cool in air at 25 ^{o}C without any disturbance. Observations with regard to gelation were recorded from time to time, and each experiment was performed in duplicate. The state of the materials was examined by the "stable-to-inversion of a test tube" method. The gels were evaluated quantitatively by determining the minimum gelator concentration (MGC) which is the minimum amount of the gelator required to form a self-supporting gel.

FT-IR Studies. The 'sol' of **1**+TA (1:1) or **2**+TA (1:1) in 10:1 t/e was drop cast on a CaF_2 cell and dried and the spectra were recorded on a Perkin-Elmer FT-IR Spectrum BX system.

Confocal Microscopy. A diluted toluene solution of the samples ($1x10^{-3}$ M) was drop cast on a pre-cleaned glass slide and it was left overnight for drying in a dust free environment. The confocal images were taken on a Leica TCS SP5 (Germany) microscope with an excitation wavelength of 458 nm.

Scanning and Transmission Electron Microscopy. The physical gel of the complexes of **1** and **2** with TA were heated to form a clear solution and carefully drop cast onto the brass stubs and were allowed to freeze-dry. The samples were then coated with gold vapor and were analyzed on a Quanta 200 SEM instrument operated at 15 kV. Diluted toluene solution of each sample was drop-cast onto a carbon coated copper grid (200 mesh size) and the TEM images were taken at an accelerating voltage of 200 kV using TECNAI T20 instrument.

Atomic Force Microscopy. A diluted toluene solution of the samples ($1x10^{-4}$ M) was drop cast on clean glass substrates. After the formation of a stable film, images were collected using an Agilent Technologies 5500 AFM instrument and the images were processed using

'Picoview 1.6' software. Non-contact mode imaging was undertaken in air using silicon cantilevers of resonance frequencies of 290 kHz and a nominal tip radius of curvature of 10-15 nm.

UV-vis and fluorescence spectroscopy. The UV-vis and fluorescence spectra of the solution were recorded on Shimadzu model 2100 spectrophotometer and Cary Eclipse (Varian) fluorescence spectrofluorimeter respectively. A peltier system was attached directly to the sample holder and the samples were equilibrated at a particular temperature before recording the corresponding spectra.

Circular Dichroism Spectroscopy (CD). Individual gel of either **1**+TA or **2**+TA was heated to form clear solution and drop cast on a quartz cell. After the formation of a uniform stable film the spectra were recorded on a Jasco J-810 CD spectropolarimeter. Contribution of the linear dichroism (LD) was excluded by recording the spectra with both the sides of the quartz cell which showed no significant changes.

Differential scanning calorimetry (DSC) of the Solids. The transition temperatures were determined for the individual complexes of **1** or **2** with TAs using a Differential Scanning Calorimeter (DSC; Perkin-Elmer, Model Pyris 1D) with heating and cooling rate fixed at 5 ^{o}C/min for all the measurements performed in the temperature range of 25-150 ^{o}C.

Polarized Optical Microscopy (POM). The morphology of the solid complexes of **1** or **2** with TAs during the thermal transitions was observed using POM. Individual solid complex was placed on a glass slide and covered using a cover-slip and the changes in their optical textures were carefully observed using polarized light microscopy (Olympus BX51) equipped with a heating stage (Mettler FP82HT) and a central processor (Mettler FP90). The heating and cooling rate was fixed at 1 ^{o}C/min for all the samples.

Quantum yield measurements. Photoluminescence quantum yield (Φ) of **1** and **2** in toluene upon excitation at 400 nm with respect to perylene (quantum yield 0.94 in cyclohexane) was estimated using the following standard equation-

$$\Phi_f = \Phi_r \, (A_r \, F_s / A_s F_r) \, (\eta_s^2 / \eta_r^2)$$

where, A_s and A_r are the absorbance and η is the refractive index. F_s and F_r represent corresponding relative integrated fluorescence intensities at a particular excitation wavelength of the sample and reference solutions respectively.

References.

[S1] B. Wang, M. R. Wasielewski, *J. Am. Chem. Soc*., 1997, **119**, 12.

[S2] S. K. Samanta, A. Pal, S. Bhattacharya, *Langmuir,* 2009, **25**, 8567.

[S3] B. R. Baker, M. H. Doll, *J. Med. Chem.,* 1971, **14**, 793.

(c) Supporting Figures and Tables

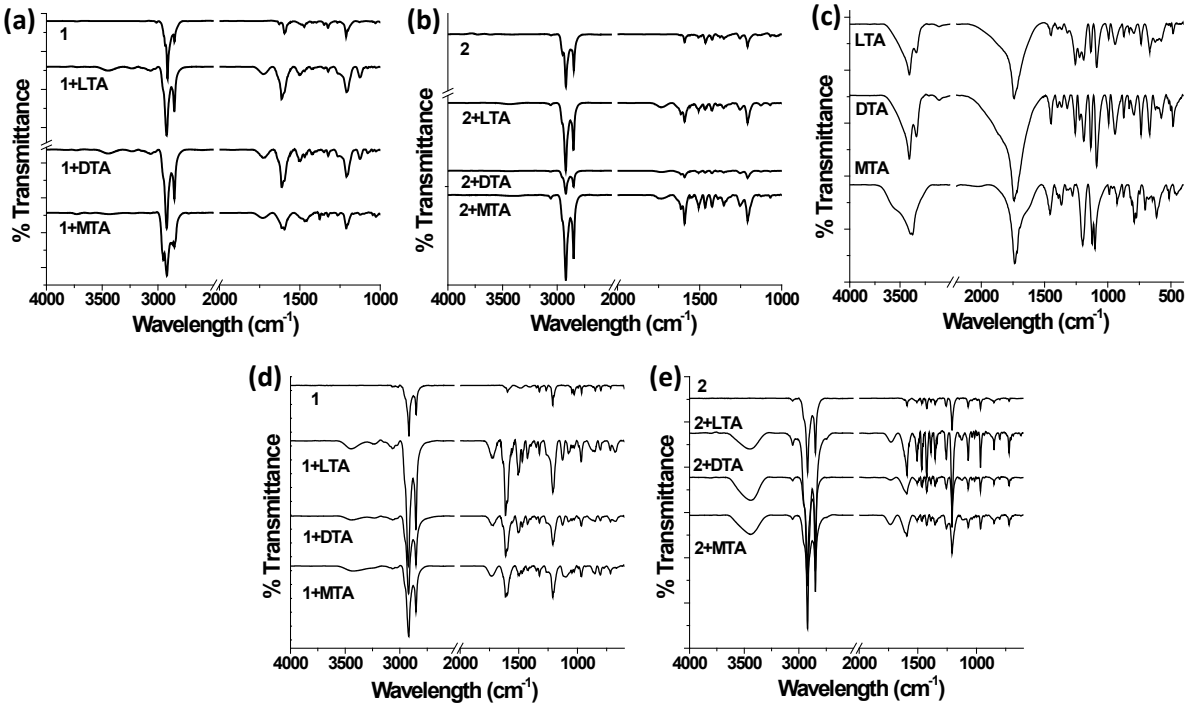

Figure S1. FT-IR spectra of (a, d) **1**+TAs (1:1) and (b, e) **2**+TAs (1:1) in the xerogels and in solids respectively and (c) three different TA in solid state.

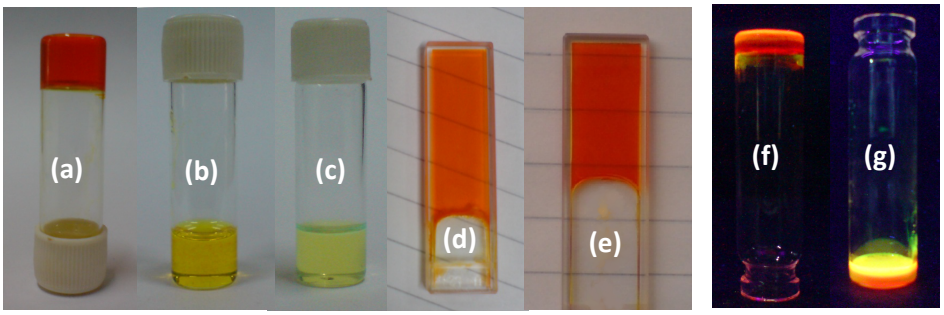

Figure S2. (a) Typical organogel of **1**+L-TA (1.15 wt%) in 10:1 toluene/ethanol mixture at 25 ^{o}C and (b) the same gel when heated to 60 ^{o}C. (c) A same concentration (1.15 wt%) of **1** alone did not form gel. Transparent nature of the gels of (d) **1**+L-TA and (e) **2**+L-TA were shown under the day light. The emission colors at (f) 25 ^{o}C and (g) 60 ^{o}C of **2**+L-TA (1.15 wt%) under 365 nm UV lamp. The ratio of the pre-gelator (*e.g.* **1**) and TA (*e.g.* L-TA) was varied to test the gelation and found that a mixture of 2:1 equiv of **1**:L-TA forms a weak gel only at higher concentrations (>3.5 wt%). Although, the mixture of 1:2 equiv (**1**:L-TA) could form efficient self-standing gel, the extra equiv of LTA was not necessary as only one equiv is sufficient to induce gelation.

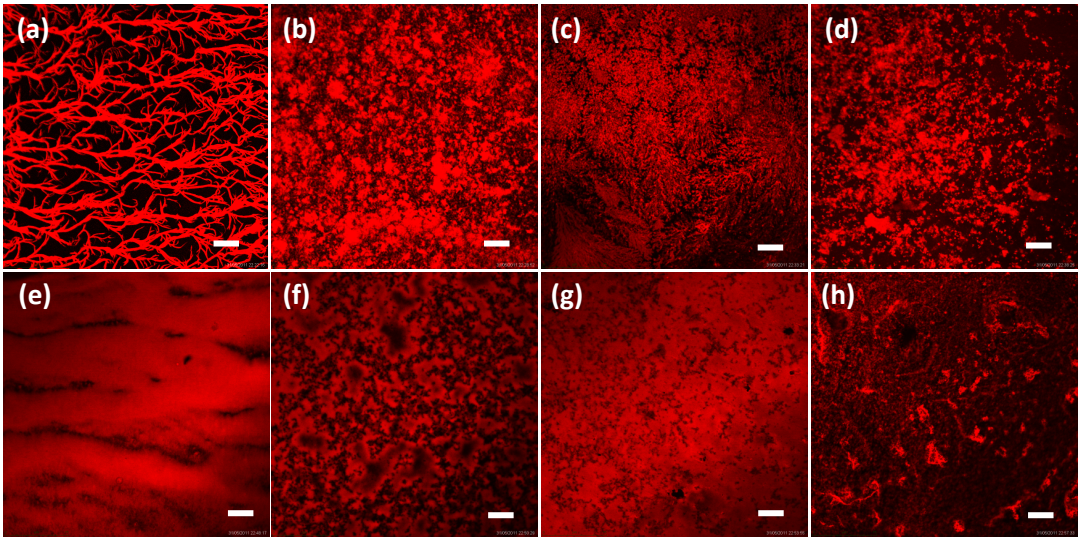

Figure S3. Confocal microscopy images of (a) **1**, (b) **1**+L-TA, (c) **1**+D-TA, (d) **1**+M-TA and (e) **2**, (f) **2**+L-TA, (g) **2**+D-TA, (h) **2**+M-TA ([**1**+TAs] = [**2**+TAs] = $1x10^{-3}$ M in 10:1 toluene/ethanol mixture, excited at 458 nm, scale bar is 20 μm in each case). The pre-gelators are luminescent in nature and they allowed us to evaluate the superstructures created by the complexes. The fibers of the pre-gelators were transformed into smaller aggregates in the TA complexes. The aggregates are the result of collation of individual fibers in a random fashion.

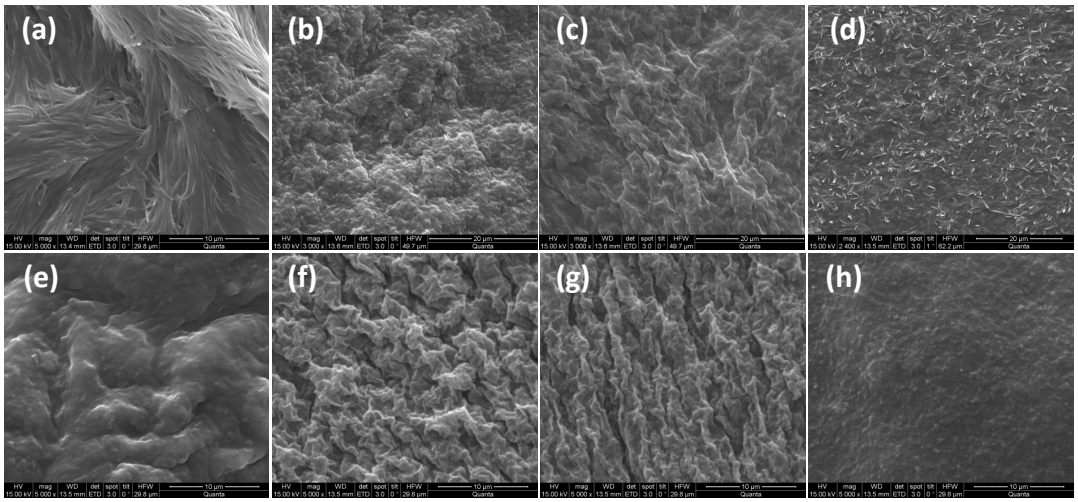

Figure S4. Scanning electron microscopic images of (a) **1**, (b) **1**+L-TA, (c) **1**+D-TA, (d) **1**+M-TA and (e) **2**, (f) **2**+L-TA, (g) **2**+D-TA and (h) **2**+M-TA. [**1**+TAs] = [**2**+TAs] = 1.15 wt% in 10:1 toluene/ethanol mixture. SEM images showed a dense thick sheet-like aggregate formation in the complexes. The aggregates could appear through the nucleation induced growth of individual fibers. The pre-gelators **1** alone showed the presence of fibrillar morphology under similar conditions. The complexes of **1** and **2** with M-TA showed different morphologies than their chiral TA counterparts.

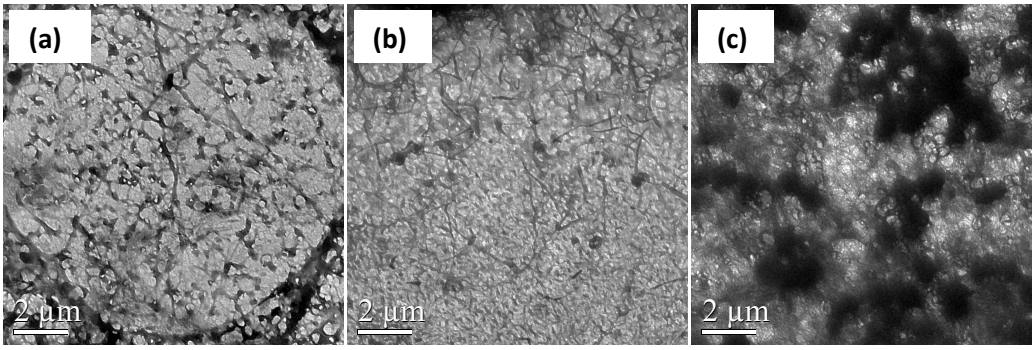

Figure S5. Transmission electron microscopic images of (a) **1**+L-TA, (b) **1**+D-TA and (c) **1**+M-TA. Concentration of the complexes was 10^{-4} M in each case. Notably, **1**+M-TA complex, which did not form gel, showed greater degree of aggregate formation although fibers still persisted.

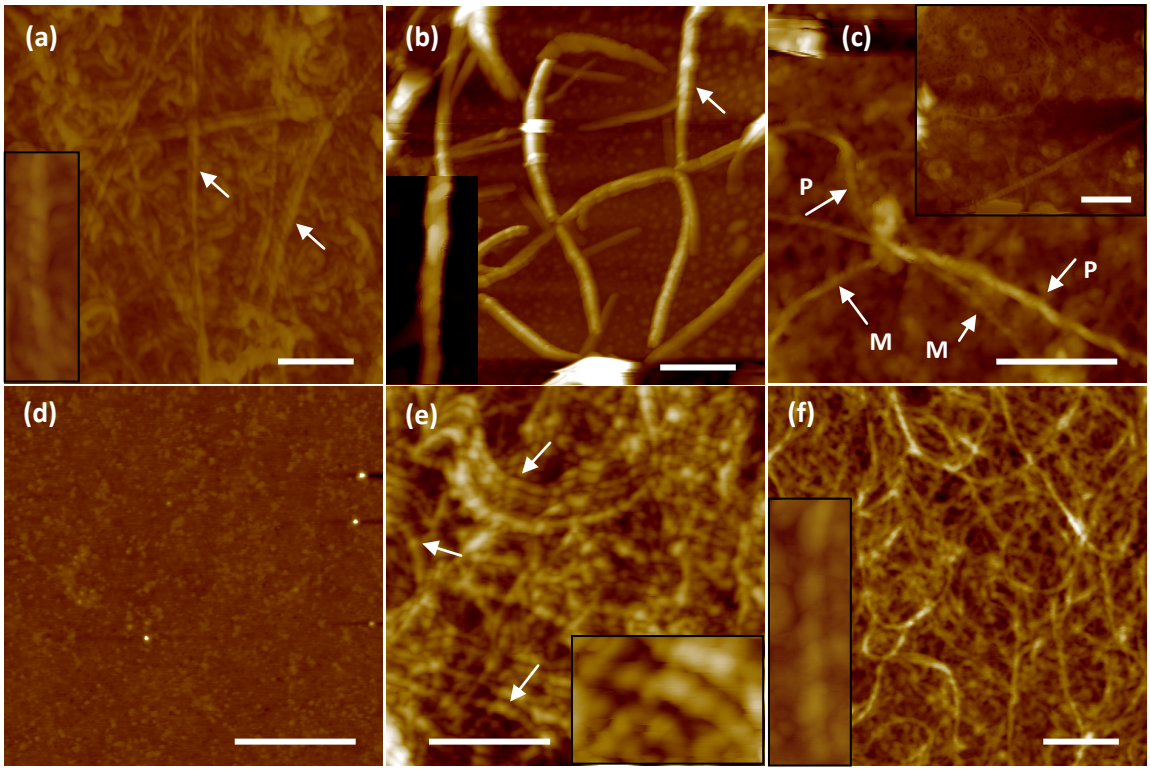

Figure S6. Atomic force microscopy topography images of (a) **1**+L-TA, (b) **1**+D-TA, (c) **1**+M-TA, (d) **1** alone, (e) **2**+L-TA and (f) **2**+D-TA. Inset in each figure showing a magnified image of the corresponding helical fibers. The arrows pointing toward the helical turns of the fibers. Scale bar is 1 um in each case. A greater extent of chiral fibers is observed in **2**+TA compared to **1**+TA complexes because of a longer conjugation and better reach for the neighbouring molecules in the assembly in **2**+TA complexes. This explains a larger CD signal (value in mdeg) in **2**+TA complexes. A similar concentration of **1** alone failed to form a fibrillar structure due to the absence of the TA molecule to anchor between the pyridine moieties.

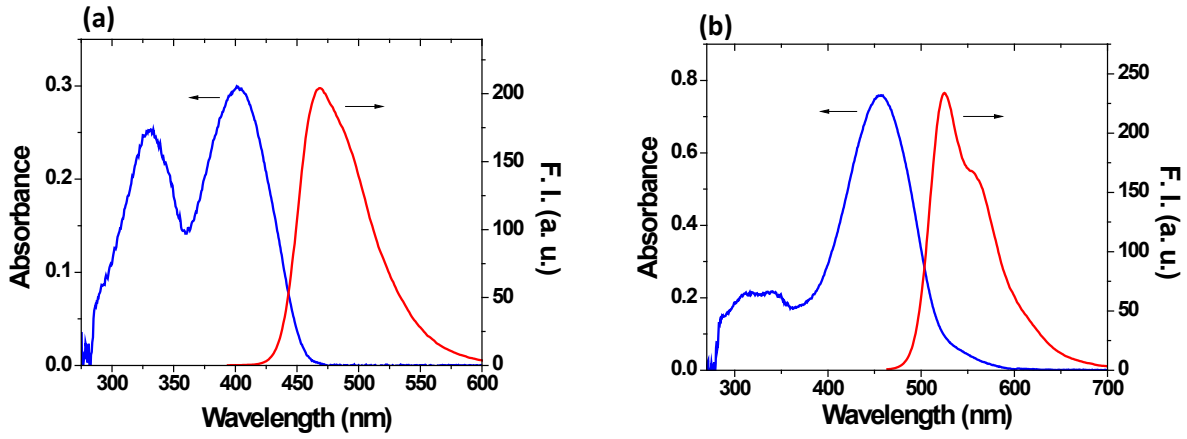

Figure S7. (a) Absorption and emission spectrum of (a) **1** and (b) **2** in 10:1 toluene/ethanol mixture. ([**1**, **2**] = 1x10^{-5} M, λ_{ex} for **1** = 380 nm and for **2** = 450 nm).

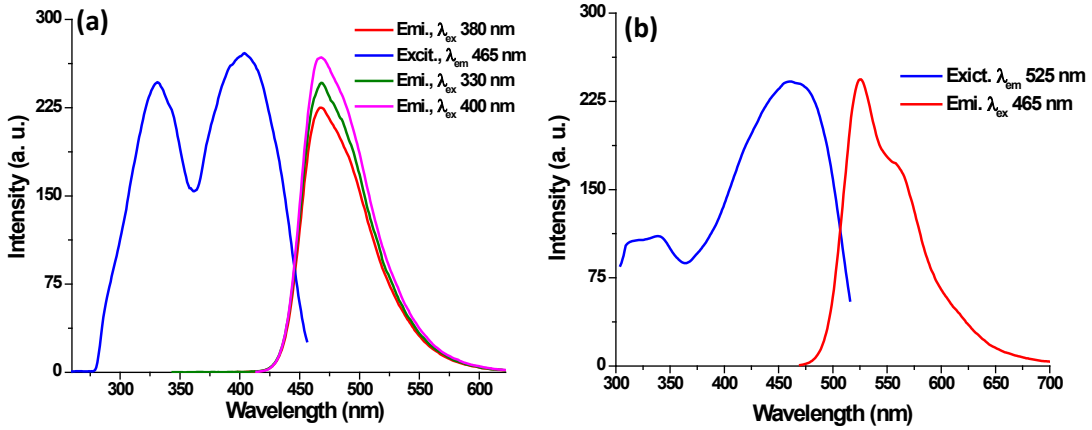

Figure S8. Excitation and emission spectrum of (a) **1** and (b) **2** in 10:1 toluene/ethanol mixture. The excitation spectrum of **1** at the emission maximum of 465 nm exhibited two bands at 330 nm and 400 nm. Excitation at any of these two maxima produced identical emission spectrum at 465 nm. ([**1**, **2**] = 1x10^{-5} M, λ_{ex} for **1** = 380 nm and for **2** = 450 nm).

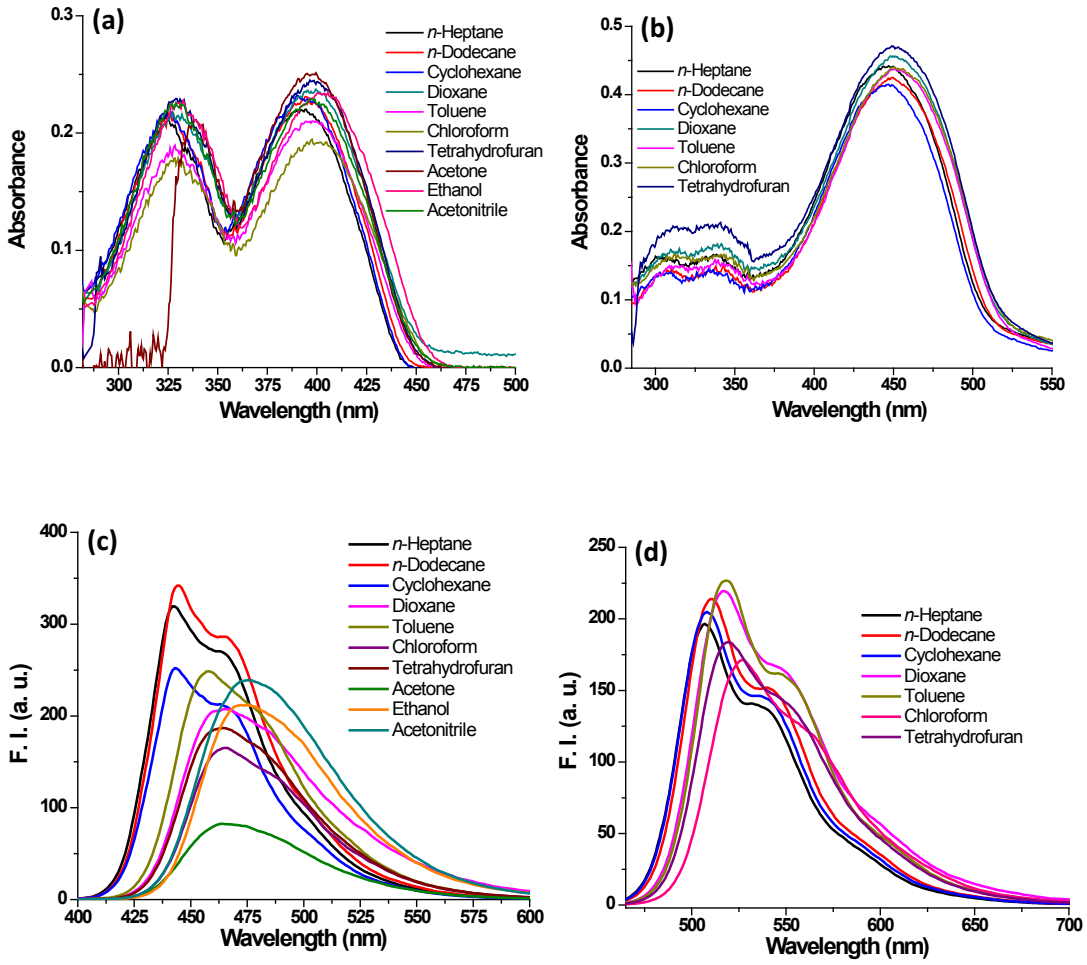

Figure S9. Solvatochromic properties of **1** and **2** in different solvents under (a, b) UV-vis and (c, d) fluorescence emission studies respectively (excitation wavelength = 380 nm for **1** and 450 nm for **2**, [**1**, **2**] = $1x10^{-5}$ M in each case). Solvatochromic shifts in the emission maximum showed on changing the solvent from *n*-heptane to chloroform a 23 nm shift occurs in **1** and a 21 nm shift occurs in **2**. However, the shifts are even greater in **1** in the solvents like acetonitrile (475 nm) and ethanol (473 nm) in which compound **2** precipitated due to having six non-polar *n*-hexadecyl chains.

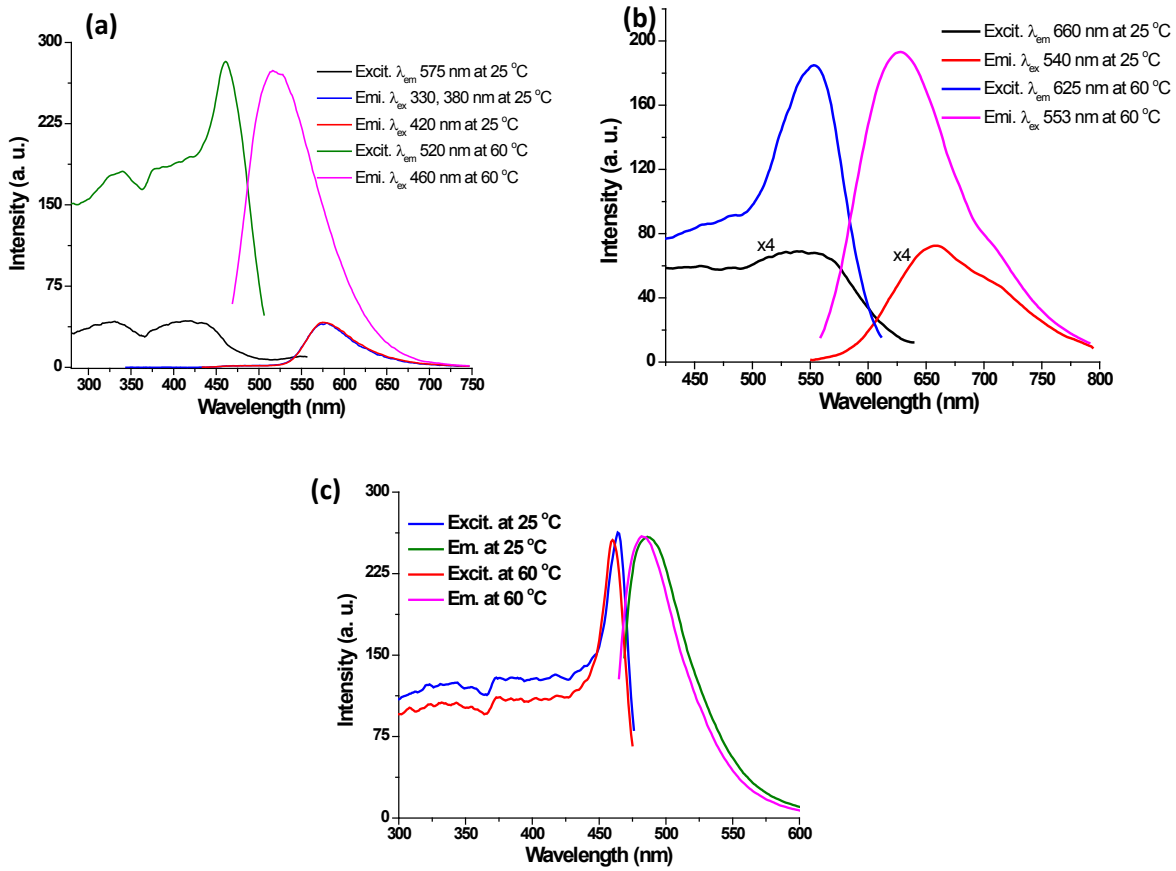

Figure S10. Excitation and emission spectra of the gel and sol of (a) **1**+L-TA (λ_{ex} = 380 nm and λ_{em} = 575 nm) and (b) **2**+L-TA (λ_{ex} = 540 nm and λ_{em} = 660 nm) in 10:1 toluene/ethanol mixture (concentration 1.15 wt% for both). The excitation spectra of **1**+L-TA at 25 °C showed two bands at 330 and 420 nm and the corresponding emission spectra at any of these two peaks showed emission with a maximum at 575 nm. At 60 °C the excitation and emission band appeared at 460 and 520 nm respectively. For **2**+L-TA, the excitation spectra at 25 °C showed a band at 540 nm and the corresponding emission spectra appeared at 660 nm. However, at 60 °C the spectra showed corresponding excitation and emission band at 553 nm and 625 nm respectively. (c) **1** alone (1.15 wt%) at 25 °C and 60 °C, (λ_{ex} = 460 nm and λ_{em} = 485 nm) in the solution in 10:1 toluene/ethanol mixture.

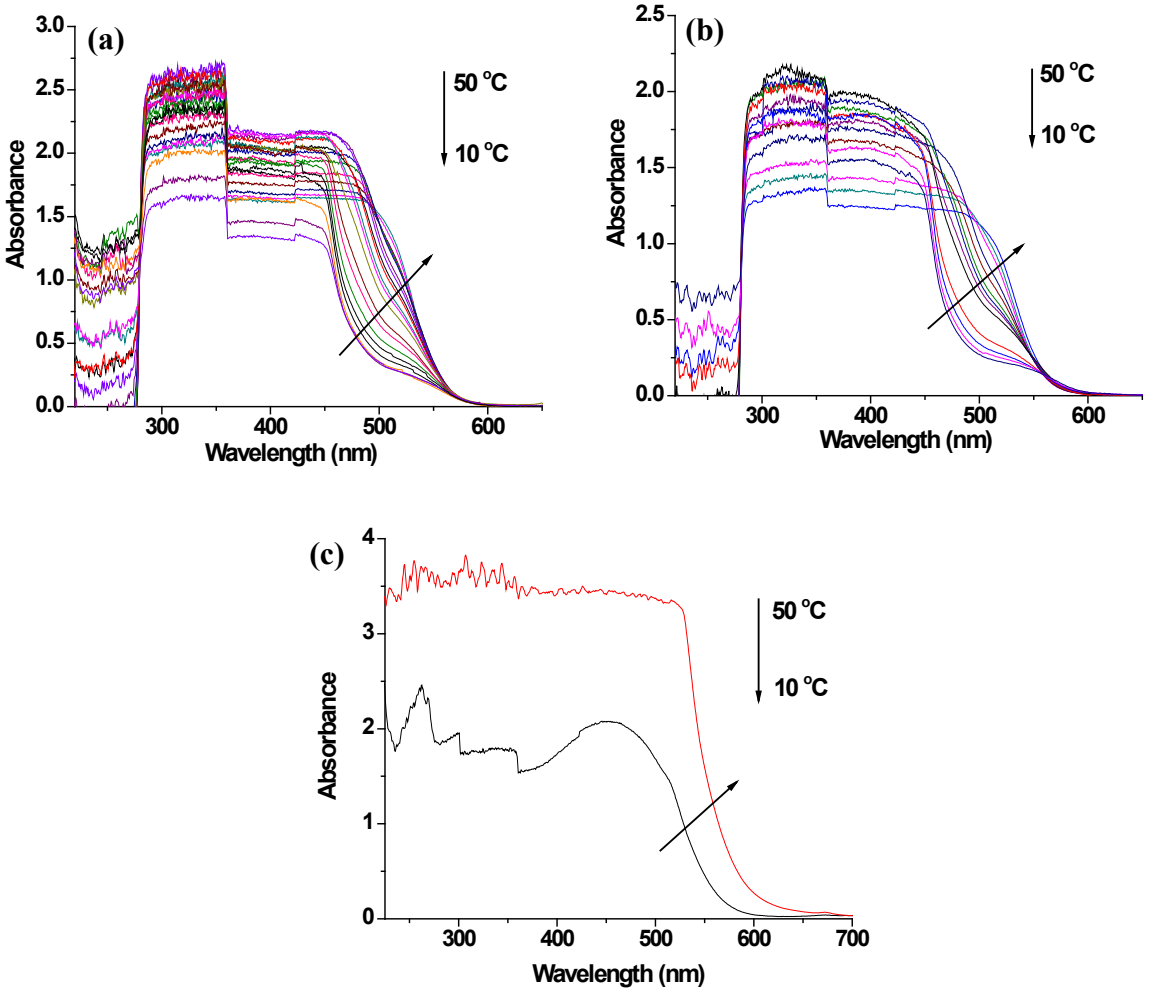

Figure S11. Temperature dependent UV-vis spectra of 1.15 wt% of each of (a) **1**+L-TA (b) **1**+D-TA and (c) **2**+L-TA in 10:1 toluene/ethanol mixture. In each case, upon cooling the sol a broad shoulder band was progressively observed (indicated by arrow) with the onset of gelation. This indicates that the gelation here is induced by a J-type aggregation.

.

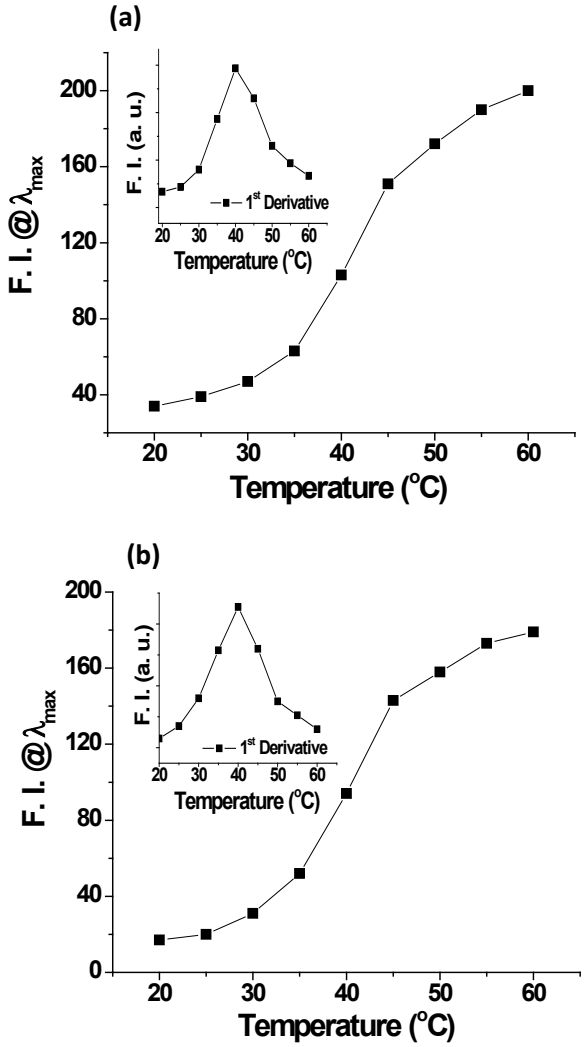

Figure S12. Plot of intensity at the emission maximum as a function of temperature for the variable temperature emission spectra of (a) **1**+L-TA gel and (b) **2**+L-TA gel. Insets showing the 1st derivative plot of the sigmoidal curves indicating that the gel-to-sol transition temperature is ~40 °C for both the gels.

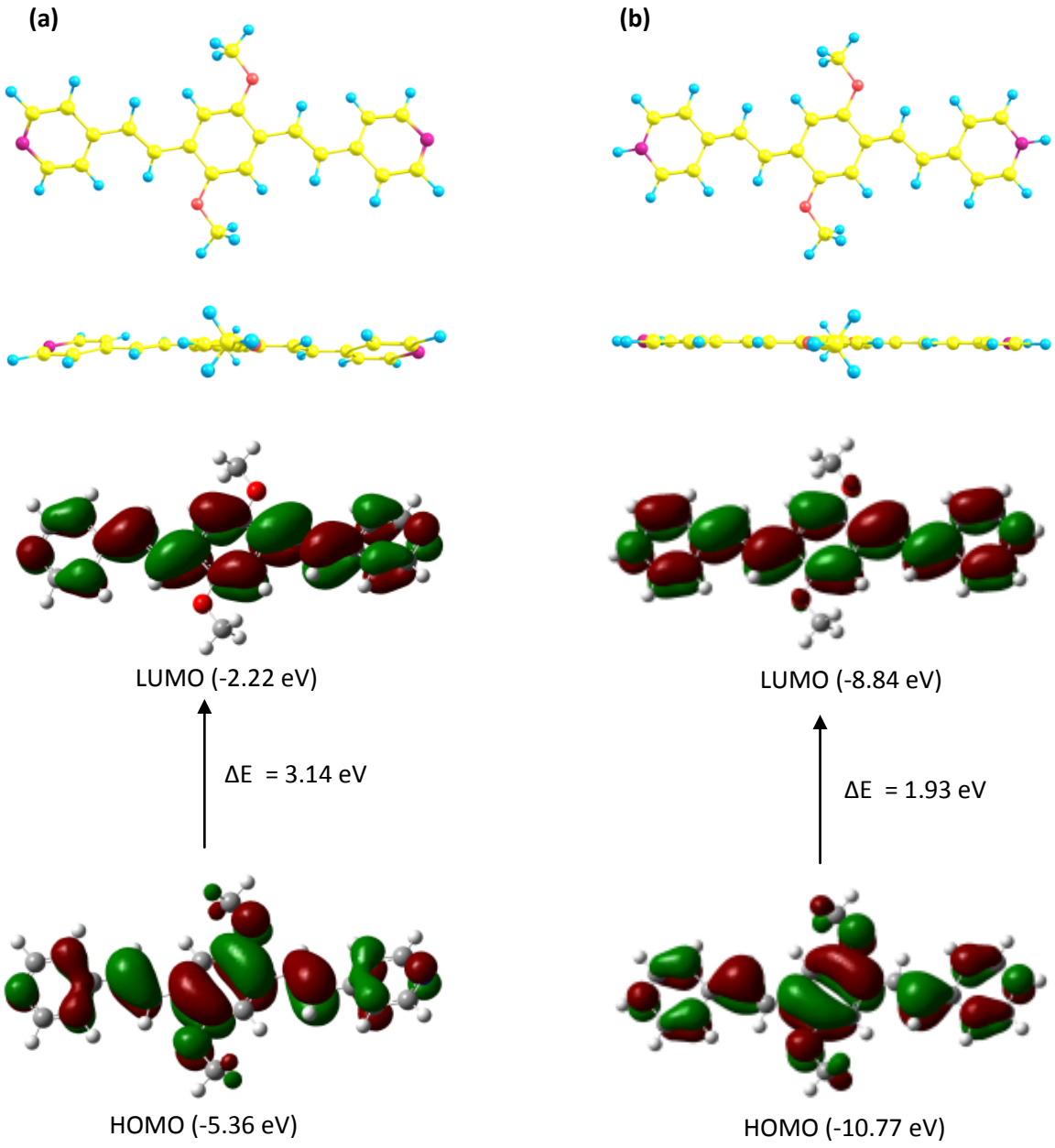

Figure S13. Energy minimized structures and the frontier molecular orbitals of (a) **1** and (b) **1**+2H$^+$ in gas-phase using B3LYP (6-31G*).

Upon protonation, both **1** and **2** attains planarity in their aromatic backbone and stabilizes the HOMO and LUMO energy levels.

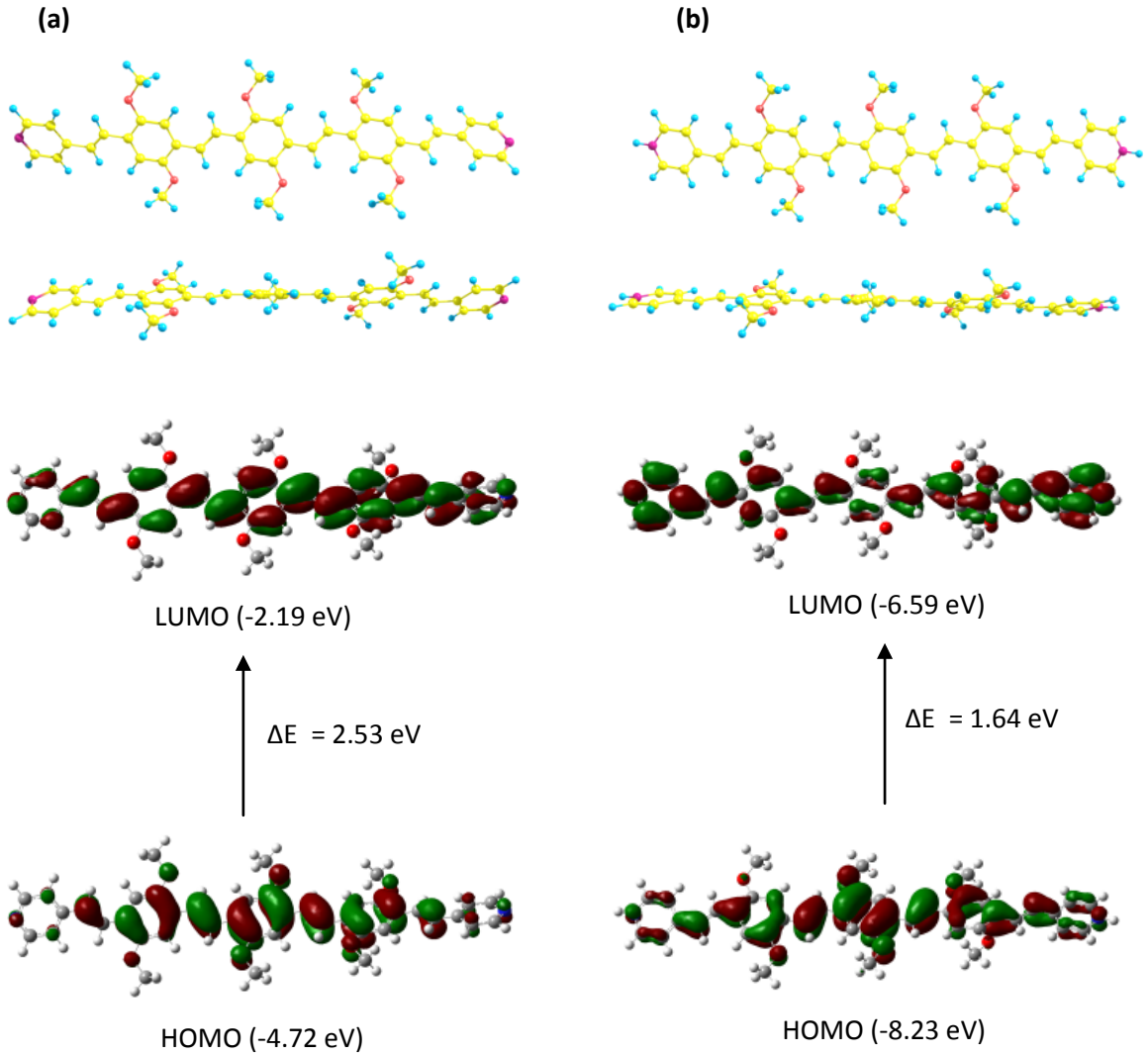

Figure S14. Energy minimized structures and the frontier molecular orbitals of (a) **2** and (b) **2**+2H$^+$ in gas-phase using B3LYP (6-31G*).

Table S1. Calculated energy levels for the frontier molecular orbitals of the energy minimized structures of **1**, **2**, **1**+2H$^+$ and **2**+2H$^+$.

	1	**1**+2H$^+$	**2**	**2**+2H$^+$
LUMO (eV)	-2.22	-8.84	-2.19	-6.59
HOMO (eV)	-5.36	-10.77	-4.72	-8.23
ΔE (eV)	3.14	1.93	2.53	1.64

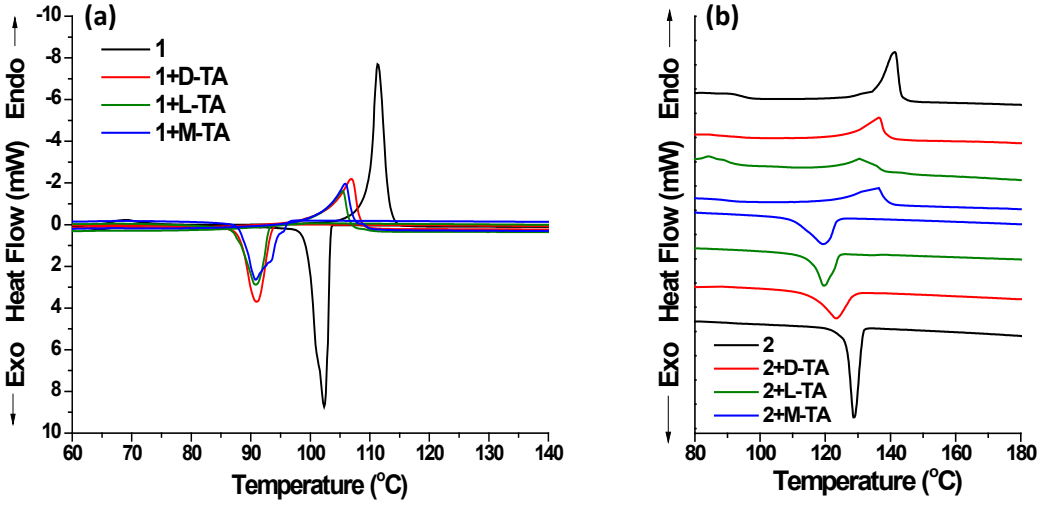

Figure S15. Solid state DSC curves for (a) **1**+TAs and (b) **2**+TAs complexes (the heating and cooling rate was fixed at 10 °C/min).

Table S2. Thermal phase-transition temperature for the melting and freezing cycles for the complexes of **1** and **2** with TA. (Error ± 0.2 °C)

	Melting (°C)	Freezing (°C)
1	113.3	102.3
1+L-TA	105.4	90.9
1+D-TA	106.9	91.0
1+M-TA	105.9	90.8
2	141.3	128.8
2+L-TA	131.0	123.5
2+D-TA	136.6	119.6
2+M-TA	136.0	119.4

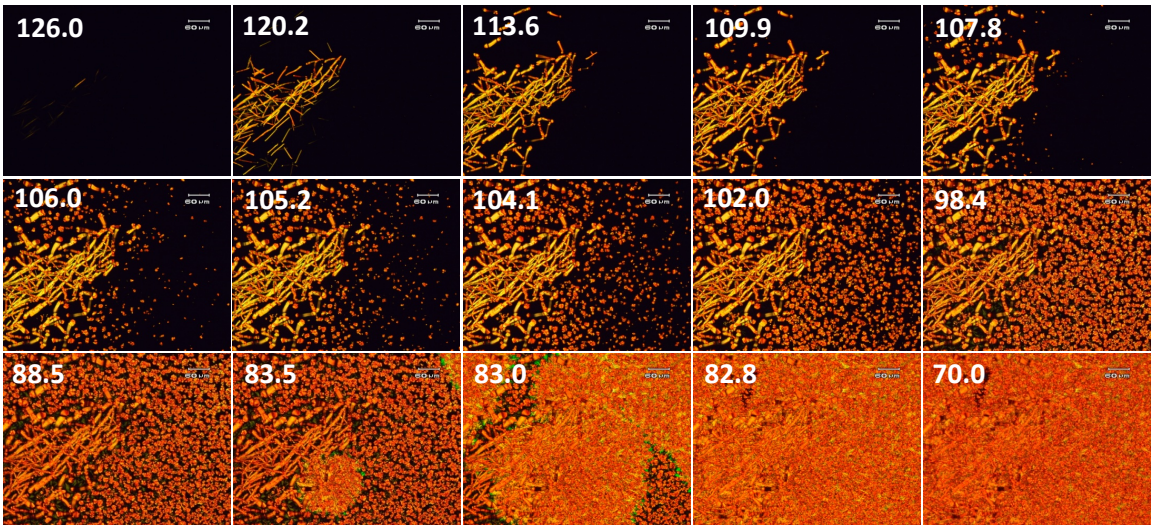

Figure S16. Snapshots of the anisotropic growth of **1**+L-TA upon progressively decreasing temperature (^{o}C) from the isotropic melt.

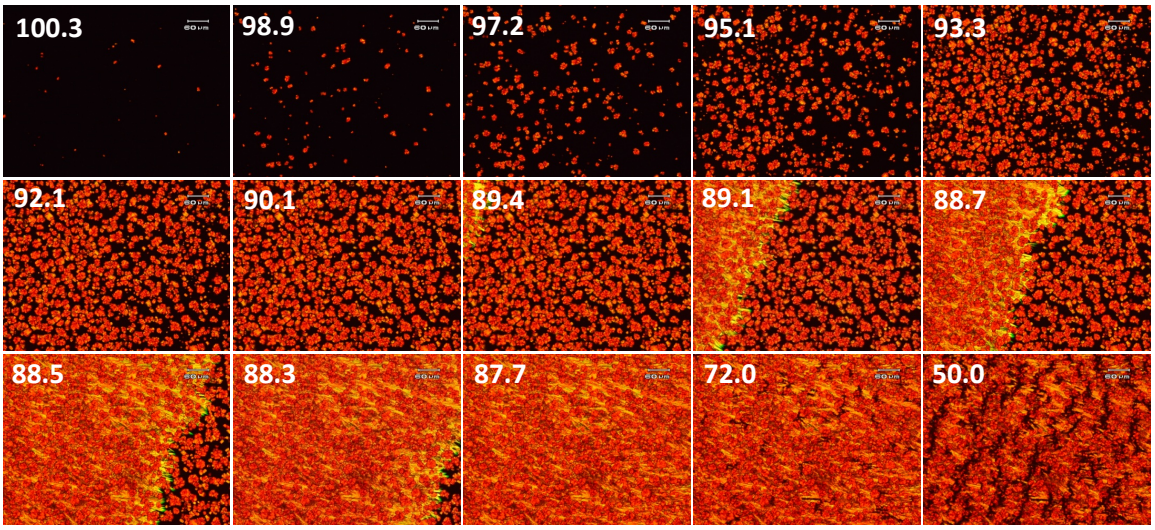

Figure S17. Snapshots of the anisotropic growth of **1**+D-TA upon progressively decreasing temperature (^{o}C) from the isotropic melt.

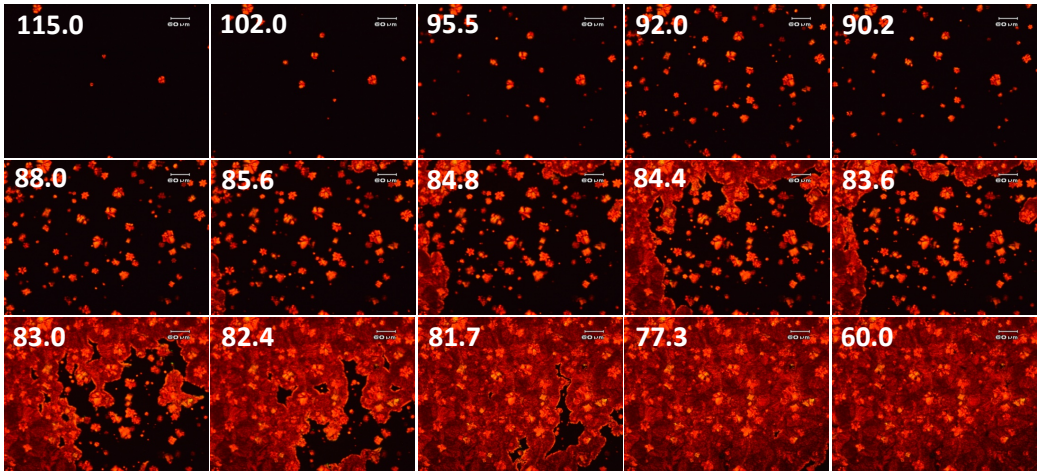

Figure S18. Snapshots of the anisotropic growth of **1**+M-TA upon progressively decreasing temperature (^{o}C) from the isotropic melt.

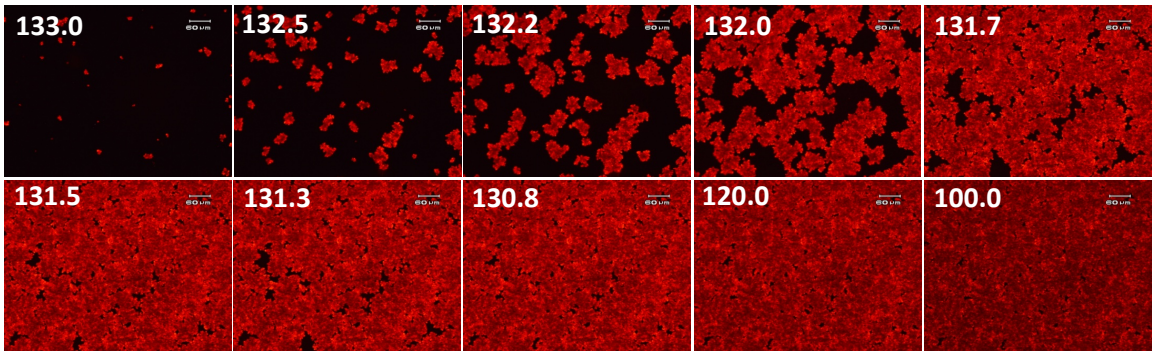

Figure S19. Snapshots of the anisotropic growth of **2** upon progressively decreasing temperature (^{o}C) from the isotropic melt.

Appearance of birefringent texture is a consequence of anisotropic growth of the gel assembly. As per the AFM images, chiral TAs produce a particular type of chiral helical morphology (right-handed in case of **1**+D-TA and left-handed for **1**+L-TA). Therefore, a similarity in the birefringent texture was observed in case of **1**+D-TA and **1**+L-TA. However, **1**+M-TA produces both left- and right-handed helical fibers as well as coil-type morphology, for which a different birefringent texture (focal conic texture) was observed along with some smaller domain morphologies (may be due to the fibers).

Although **2** alone exhibited a liquid-crystalline behavior, in case of the complex of **2**+TA, the liquid-crystalline behavior of **2** was not observed. However, there is a similarity in the birefringent textures of **1**+M-TA and **2**+M-TA which indicates that a similar type of supramolecular assembly may be responsible for the formation of such mesophases.